ESTABLISHMENT OF A NON-PERMANENT GPS NETWORK TO MONITOR THE RECENT NE-SW DEFORMATION IN THE GRANADA BASIN (BETIC CORDILLERA, SOUTHERN SPAIN)

A.J. GIL[1], G. RODRÍGUEZ-CADEROT[2], M.C. LACY[3], A.M. RUIZ[1], C. SANZ DE GALDEANO[4], P. ALFARO[5]

ABSTRACT

The Granada Basin (Central Betic Cordillera), one of the most seismically active areas of the Iberian Peninsula, is currently subjected to NW-SE compression and NE-SW extension. The present day extension is accommodated by normal faults with various orientations but particularly with a NW-SE strike. At the surface, these active NW-SE normal faults are mainly concentrated on the NE part of the Basin. In this part we have selected a 15-km long segment where several active normal faults crop out. Using the marine Tortonian rocks as a reference, we have calculated a minimum extensional rate of 0.15-0.30 mm/year. The observed block rotation, the listric geometry of faults at depth and the distribution of seismicity over the whole Basin, indicate that this rate is a minimum value. In the framework of an interdisciplinary research project a non-permanent GPS-network has been established in the central sector of Betic Cordillera to monitor the crustal deformations. The first two observation campaigns were done in 1999 and 2000.

Keywords: Active Tectonics, GPS network, crustal deformation, Betic Cordillera.

1. INTRODUCTION

The Granada Basin, in the central sector of the Betic Cordillera (southern Spain), extends some 60 km E-W and 40 km N-S (Fig. 1). This intramountain Basin, which originated during the Late Miocene, is filled by Upper Miocene, Pliocene and Quaternary rocks deposited over a basement composed, in the north, of rocks of the External Zone of the Cordillera, and in the south, of the Internal Zone. The study area includes three complexes of the Internal Zone, namely the Malaguide, Alpujarride and Nevado-Filabride (Fig. 2).

1 Dept. Ing. Cartográfica, Geodésica y Fotogrametría. E.P.S., Universidad de Jaén, Virgen de la Cabeza 2, 2371 Jaén, Spain (ajgil@ujaen.es)

2 Dept. Astronomía y Geodesia, Universidad Complutense de Madrid, Ciudad Universitaria s/n, 28040 Madrid, Spain (gracia@mat.ucm.es)

3 Facoltà di Ingegneria di Como, Instituto Politecnico di Milano, Via Valleggio 11, 22100 Como, Italy (clara@torno.ing.unico.it)

4 Instituto Andaluz de Ciencias de la Tierra, Facultad de Ciencias, 18071 Granada, Spain (csanz@ugr.es)

5 Dept. Ciencias de la Tierra, Universidad de Alicante, San Vicente del Raspeig, Alicante, Spain (pedro.alfaro@ua.es)

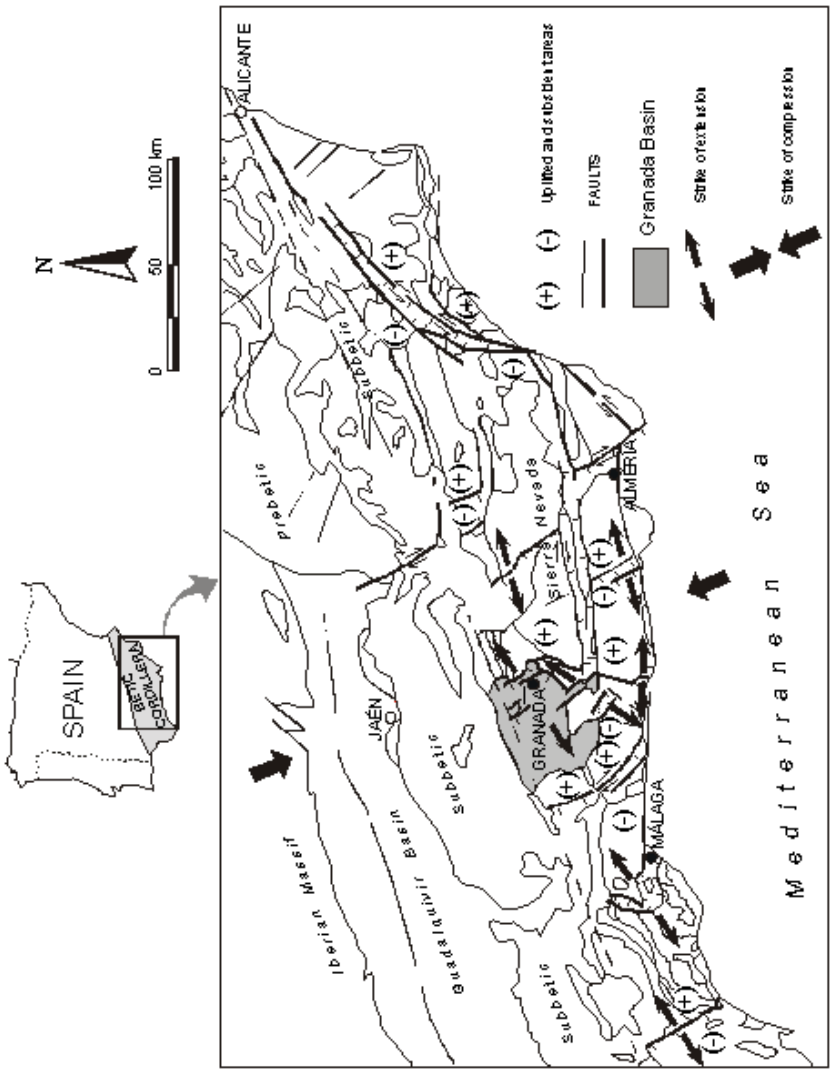

Fig. 1. Simplified geological map of the Betic Cordillera showing the location of the Granada Basin. The orientation of the present extension, compression the uplifted and subsided sectors are shown.

This Basin is one of the most seismically active areas of the Iberian Peninsula. Small-magnitude earthquakes ($m_b < 5$) characterise the instrumental seismic activity for the region (*Morales et al., 1997*), but the occurrence of moderate-high magnitude seismic events is revealed by the existence of various historic earthquakes (*Vidal, 1986*). The Andalusia earthquake (1884) was the most recent catastrophic earthquake recorded in the Iberian Peninsula, with a maximum M.S.K. intensity of *X* and an estimated *Ms* magnitude of 6.5 − 6.7 (*Muñoz and Udías, 1991*). In addition to this historical evidence, there are also proofs of similar moderate to high-magnitude earthquakes having occurred in the Basin over the last few million years, from at least the Late Miocene. This fact is deduced by the presence of various Upper Miocene-Pliocene layers of seismites in the sedimentary fill of the Granada Basin (*Rodríguez-Fernández, 1982*). In addition, *Alfaro et al. (2001)* identified several Paleoseismic events in Late Pleistocene-Holocene detritic sediments in the southeastern sector of the Basin.

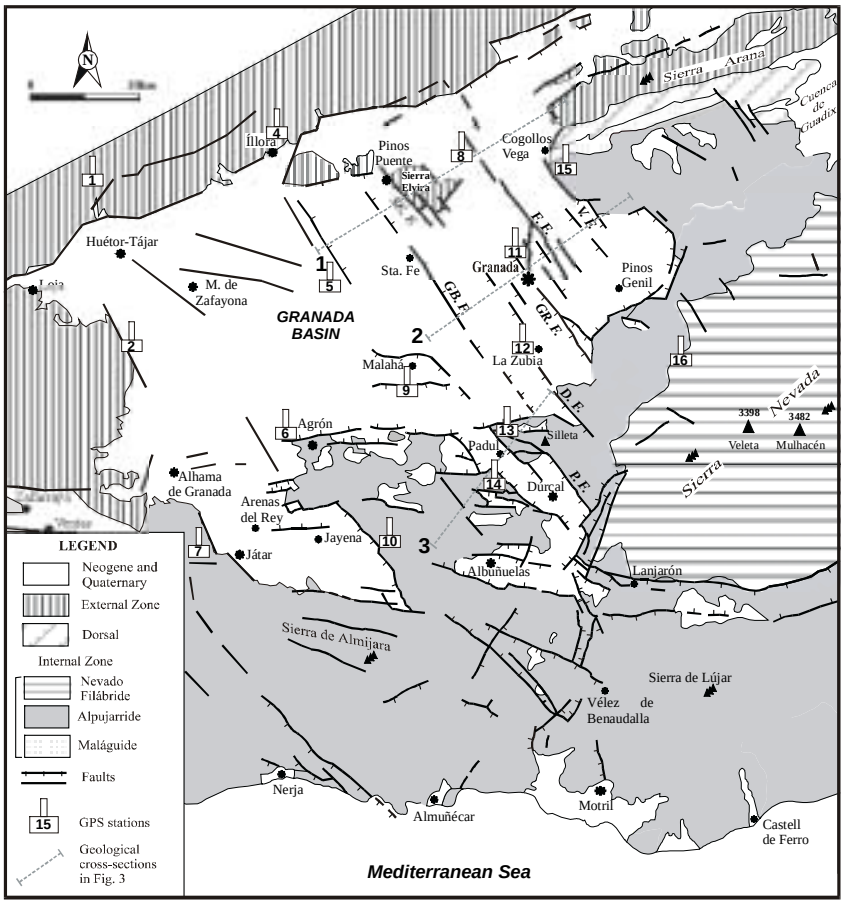

Fig. 2. Geological map of the Granada Basin with location of the geological cross-sections of Fig. 3 and the GPS stations.

The seismic activity of the Granada Basin is linked to the collision of the Eurasian and African plates. These plates converge at a rate of approximately 5 mm/y (*Argus et al., 1989; DeMets et al., 1994*). Both the geological structure and the analysis of focal mechanisms indicate a complex regional stress field in the upper crust of the central Betic Cordillera. From a geodynamic point of view the Basin is currently subject to a compressive stress field running NW-SE with an associated NE-SW extension (*Galindo-Zaldívar et al., 1999*).

From the Late Miocene to the present the NW-SE compression has been mainly accommodated by the folding of the basement and the Upper Miocene-Quaternary sedimentary cover. The most notable of these folds is the E-W Sierra Nevada anticline (*Fontboté, 1957; Galindo-Zaldívar et al., 1996*), which affects the basement of the Internal Zone of the Betic Cordillera.

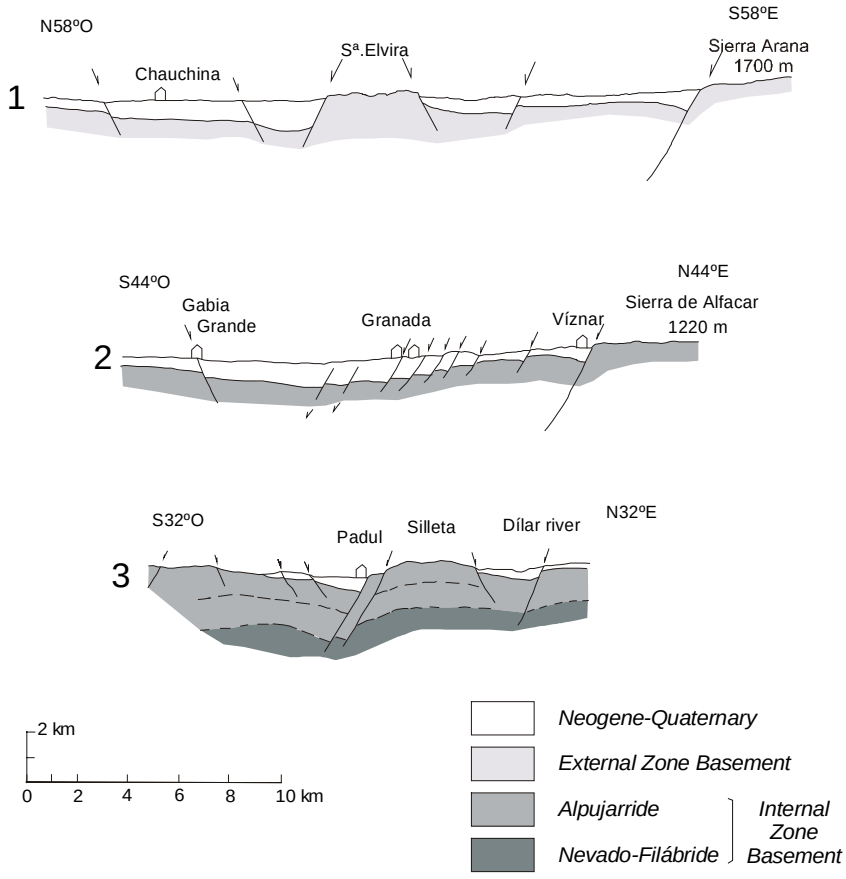

Fig. 3. Geological cross-sections along the eastern sector of the Granada Basin. See location in Fig. 2.

The extension has been described for several parts of the Betic Cordillera (*Galindo-Zaldívar et al., 1989,1996; García-Dueñas et al., 1992; Crespo-Blanc et al., 1993a,b*) (Fig. 1). Using information about the seismicity distribution at depth, *Galindo-Zaldívar et al. (1999)* deduced that the main level of compensation of these extensional faults is located at approximately 9 to 16 km depth in the NE of the Granada Basin, whilst it is progressively deeper towards the west, between 20 and 25 km depth in the SW sector of the Basin. In addition to this main detachment, there are others closer to the surface, such as the contact between the Alpujarride and Nevado-Filabride. This tectonic contact was originally a thrust and subsequently operated as a large gravitational slide (*Galindo-Zaldívar et al., 1996; Martínez and Azañón, 1997*). Nevertheless, this extensional detachment is cut by high-angle or vertical faults in the SE of the study area close to Lanjarón (*Sanz de Galdeano and López-Garrido, 2000*).

In addition to the NW-SE shortening and the NE-SW extension, the active folding and the active NW-SE normal faults are also responsible for vertical movements in the Basin. *Sanz de Galdeano and López-Garrido (2000)* indicate that from the Late Miocene to the present, in the eastern part of the Granada Basin, the whole vertical displacement is more than 5000 m. Based on the different elevations of Neogene and Quaternary sediments, *Sanz de Galdeano (personal communication, 1996)* and *Keller et al. (personal communication, 1996)* estimated an average rate of uplift for the western Sierra Nevada of between 0.4 and 0.6 mm/y, occasionally reaching 0.8 mm/y.

In spite of the evidence for present-day tectonic activity based on regional seismicity and geological features, the present NE-SW extension rates in the Granada Basin has yet to be determined. In this study, we have calculated the deformation of the main NW-SE normal faults using the marine Tortonian rocks as a reference. From the different elevations of these rocks cut by faults, we have estimated the total throw in the study area and the average NE-SW extension that has occurred in the Basin from the Late Miocene to the present. In addition, and in order to quantify the present deformation at the Granada Basin, a GPS monitoring network of 15 points was set up (Fig. 2). In this article we describe the main features of the GPS network and the geodetic results obtained in the first two surveys made in February 1999 and June 2000. Results from future surveys will be compared to those suggested by geological observations.

The first objective of the GPS network is to confirm the horizontal deformation, NW-SE shortening and NE-SW extension, that has been deduced from the analysis of focal mechanisms and structural data. The second one is to quantify present rates of horizontal deformation, identifying sectors with the greatest deformation and the third one is to quantify vertical deformation or relative uplift between different blocks of the study area.

2. RECENT NE-SW EXTENSION COMPUTATION IN THE GRANADA BASIN

From the Late Miocene to the present the NE-SW extension was accommodated by normal faults with various orientations, but particularly with a NW-SE strike (Fig. 3). At the surface, these active NW-SE normal faults are mainly concentrated on the north-eastern part of the Basin, which coincides with the western border of the Sierras Arana, Alfacar and Nevada. These NW-SE faults exhibit numerous signs of recent activity (fault scarps, triangular facets, deformed alluvial fans, etc.) (*Lhénaff, 1965; Estévez and Sanz de*

Galdeano, 1983; Riley and Moore, 1993; Calvache et al., 1997; Sanz de Galdeano and López Garrido, 1999).

In this area of the Basin, we have selected a segment 15 km long which extends from Sierra Alfacar to Sierra Elvira and is perpendicular to the NW-SE faults (Fig. 4). Within this sector the Víznar, Fargue, Granada and Sierra Elvira-Dílar faults have caused subsidence of several blocks to the west, producing topographic steps (*Estévez and Sanz de Galdeano, 1983*) (Fig. 4). Those NW-SE faults dip towards the SW, with the exception of several conjugate faults (e.g. Gabia fault) that dip to the NE. These conjugate faults generate several grabens, such as the one of Granada.

The Víznar fault located at the northeastern extreme of the studied segment, produces a contact between sedimentary and metamorphic rocks of the Internal Zone basement with detritic rocks from the Late Miocene-Quaternary. Although the Víznar fault cuts Quaternary deposits, its main activity was during the late Miocene and Pliocene, as can be deduced from syntectonic deposits related to the fault. The Fargue and Granada faults cut alluvial rocks of the Alhambra Formation dating from the Pleistocene. The Sierra Elvira-Dílar fault has a clear expression at the surface at both its NW and SE extremes (Sierra Elvira and Dílar segments, respectively). In the studied segment, the Sierra Elvira-Dílar Fault is not visible because is covered by recent Quaternary deposits and this area is used intensively in agriculture. In addition, there are other NW-SE normal faults, with a lower slip, which also accommodate part of the NE-SW extension that has arisen in this sector of the Basin (Fig. 4).

The marine Tortonian rocks are located at different elevations along this segment, because of the vertical displacement of these active NW-SE normal faults. In the small Basin situated to the west of the Sierra Elvira, they are found at their lowest elevation (– 600 m), deduced from geophysical data, while in the Sierra de Alfacar they outcrop at

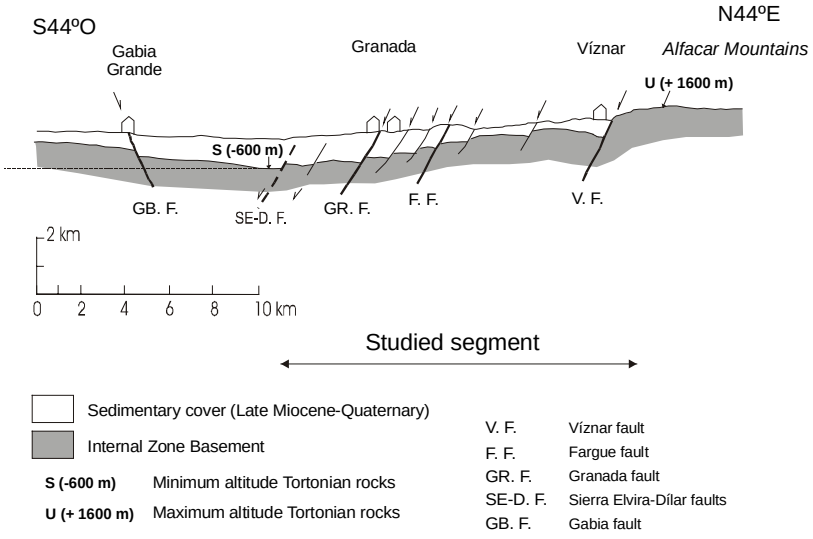

Fig. 4. Geological cross-section of the segment where NE-SW extension rate has been calculated.

up to 1200 m in the hanging wall of the Víznar fault. In the footwall, where the topography of the Sierra de Alfacar exceeds 1600 m, these marine materials have been eroded. In the Sierra Arana, located just to the North, the Tortonian marine rocks outcrop at 1623 m. We assume that, as minimum, the Tortonian rocks reach 1600 m at Alfacar Mountains (Fig. 4). Using the marine Tortonian rocks as a stratigraphic marker, we deduced a minimum total throw of 2200 m along the studied segment. To the SE of the Granada Basin, the deposition of the Pinos Genil formation or Block formation, late Tortonian in age, indicates significant uplift and intense erosion in the Sierra Nevada. This formation, marine at its base, comprises large pebbles and boulders several cubic metres in size. Based on these observations, we assume that the 2200 meters minimum throw estimated in the studied area started 7 or 8 My ago (late Tortonian).

At the surface, most of these normal faults have high-angle dips (between 45º and 60º). Taking into account an average dip varying between 45º and 60º and a dip slip movement along fault planes deduced from slickensides, the NE-SW extension will be half of the total throw for 60º dipping faults and similar to the total throw for 45º dipping faults. Thus, the total extension produced between the Tortonian and the present ranges at least between 2200 m and 1100 m. Along the 15-km segment studied the Basin was extended at a minimum rate of 0.15 – 0.30 mm/year.

This extensional rate of the Granada Basin is a minimum value since: (a) based on the distribution of the seismicity over the whole Basin (*Morales et al., 1997*), this NE extension is not exclusively limited to the study sector, (b) the rotation of blocks and the listric geometry of some fault planes imply a greater extension. In the study area, the NW-SE faults have a probable listric geometry (*Galindo-Zaldívar et al., 1999*) which could have their origin in the main extensional detachment in the region, located between 9 and 16 km deep, where seismicity is concentrated (*Morales et al., 1997; Galindo-Zaldívar et al., 1999; Sanz de Galdeano and López-Garrido, 2000*). Other minor NW-SE faults probably have a shallower origin in more superficial detachments such as the Nevado-Filabride/Alpujarride contact (*Galindo-Zaldívar et al., 1999*). Besides, rotation of large and small blocks is also recognised. Using the Tortonian rocks of Sierra Arana as a reference we deduce a tilting of at least 8º. In addition to this rotation of large blocks such as the Sierra Arana, we also observe rotation of smaller-sized blocks. For example, in Víznar, the Upper Miocene and the Plio-Quaternary dip 15º towards the east, against the fault.

Summing up, along the study segment we observe that block rotation has occurred at different scales, faults have listric geometry and seismicity is distributed over the whole Basin. Consequently, the calculated rate of extension (0.15 – 0.3 mm/year) indicates a minimum rate in the 15-km long segment examined. In order to monitor the NW-SE shortening and the NE-SW extension a GPS network has been established in the Granada Basin.

3. ESTABLISHMENT OF A MONITORING GPS NETWORK

With the aim of quantifying the deformation that is currently occurring in the Basin, the first non-permanent GPS network of this area was designed (Fig. 2). For the determination of very small crustal movements using geodetic measurements, the best

option is a network of permanent GPS stations. However, when this is not possible due to financial constraints, the network of closely-spaced pillars and its periodic observation by GPS campaigns spaced over time becomes the best option (*Betti et al., 1999*).

The design of the network as well as the individual site selection required consideration of geoscientific, logistical and observational aspects (*Klotz and Lelgemann, 1999*). As a geodynamic network is considered a very long-term project the monumentation should guarantee the reoccupation after a time span. This network is made up of fifteen reinforced concrete pillars anchored to rock. Moreover, to assure that the antennas will be placed exactly at the same position in different reoccupations, the pillars have an embedded forced centring system. Nine out of the fifteen monitoring points are located over the basement rocks in the External and Internal Zones of the Cordillera that surround the Granada Basin. The remaining six points are located within the depression, over rocks of various ages.

Figure 2 shows the geological aspects of Granada Basin and GPS sites. The sites #5, #6, #9, #11 and #12 are located in the centre of the Basin, over the "relative" subsidence sectors of the Granada Basin. The others are distributed over the uplifted relief, which surround the Basin. Sites #13 and #14 are closer in order to establish a local control of the Padul normal fault, one of the most active and spectacular faults of the Basin. Site #16, the highest control point, is located in Sierra Nevada, over the Internal Zone basement in the area with apparent maximum uplift. All sites met the following requirements: no obstruction above 15 degrees; no high power lines nearby; easily accessible. New sites #22 and #25 were built in a restricted area for the second observation campaign after sites #12 and #15 were destroyed wildly.

The first survey was carried out from February 27 to March 7, 1999, and the second one from June 18 to June 25, 2000. The GPS constellation was tracked for eight-hour sessions over baseline lengths ranging from 10 km to 55 km. The equipment used was three Leica SR399 and two Leica SR9500 dual frequency carrier phase GPS receivers which belong to University of Jaen.

The network has been tied to the IGS sites Villafranca (Madrid) and San Fernando (Cádiz), from which the coordinates of the network central point were computed. GPS data processing was performed using Bernese 4.0 software (*Rothacher et al., 1996*) computing single sessions in multibaseline mode. The first step (preprocessing) related to receivers clocks calibration, performed by code pseudoranges, and detection and repair of cycle slips and removal of outliers, was carried out simultaneously for *L1* and *L2* data. The final solution for each session was obtained using the iono-free observable with precise ephemeris and antenna phase centre variation files. The coordinates of the stations, apart from a fixed reference site (#5), and relative integer ambiguities were estimated in both campaigns. Troposphere parameters were not estimated because the root mean square errors of coordinates and residuals were smaller than in a data process with estimation of these parameters. This means the final adjustment procedure did not contain clock parameters, orbital elements and atmosphere parameters. From these results we have used an intermediate program to produce GPS baselines with their covariance matrixes. Using the NETGPS program that performs the adjustment of GPS baselines accounting for their full covariance matrixes, the minimal-constrained network adjustment was done. This adjustment suddenly raised the problem of incorrect stochastic model and pushed towards its reestimation, taking into account the reliability of the network. It is

Table 1. Minimum constrained adjustment parameters (1999 and 2000 campaigns).

Ses	Eq	Unk	Red	σ_0^2	χ^2_{exp}	χ^2_{teo}	RMS *X*	RMS *Y*	RMS *Z*	S_{min}	S_{maj}	*CI*
8	90	42	48	1.16	65.08	65.17	6	3	5	7	12	14
8	93	42	51	1.15	67.63	68.67	6	3	5	4	15	14

Ses: sessions, Eq: Number of equations, Unk: unknown parameters, Red: redundancy, σ_0^2 : unit weight variance; χ^2_{exp}: experimental χ^2 with "redundancy" degrees of freedom; χ^2_{teo} theoretical χ^2 with "redundancy" degrees of freedom at the 95% confidence level; RMS: average SQM values in mm, S_{maj}: semimajor axis of the 95% confidence ellipse in mm. S_{min}: semiminor axis at the 95% confidence level in mm; CI: 95% confidence height interval in mm.

well known that the longer the baselines estimated from GPS observation are, the greater the estimate biases due to some possible mismodelling effects affecting these observations are (e.g. residual troposphere effect). Therefore, since GPS phase model may not be completely correct, the covariance matrix of GPS baselines is often underestimated. So, this covariance matrix cannot be a correct stochastic model for the GPS network adjustment and it needs to be aposteriori reestimated. The appropriate software was developed. The reestimation procedure caused some changes both in coordinates and in their covariance matrix, whose estimates are biased when wrong stochastic models are used. The discrepancies in the covariance matrix are particularly relevant with respect to the subsequent significance analysis of coordinates differences; moreover internal and external reliability are remarkably underestimated.

Figures 5 and 6 show the error ellipses of the minimum constrained network adjustment in 1999 and 2000 campaigns and Table 1 some statistical data.

Table 1 shows also that the mean precision in height is remarkably worse than in horizontal position. The difference is due to the weakness of the GPS height determination.

4. TESTING THE COORDINATES DIFFERENCES

The definition of a test to compare two GPS networks is based on the assumption that the observations, cartesian components of the GPS baselines, the coordinate estimates and their differences are normally distributed. The significancy of the coordinate differences is tested by the well-known statistic:

$$\frac{\delta \hat{x}^t Q_{\delta\delta}^{-1} \delta \hat{x}}{m \hat{\sigma}_0^2} = F_{sp}\,, \tag{1}$$

where $F_{sp} \approx F_{m,(r_1+r_2),\alpha}$ if H_0: $\hat{x}_1 = \hat{x}_2$ is true; m is the number of tested parameters. If :

$$F_{sp} \le F_{m,(r_1+r_2),\alpha} = F_t\,, \tag{2}$$

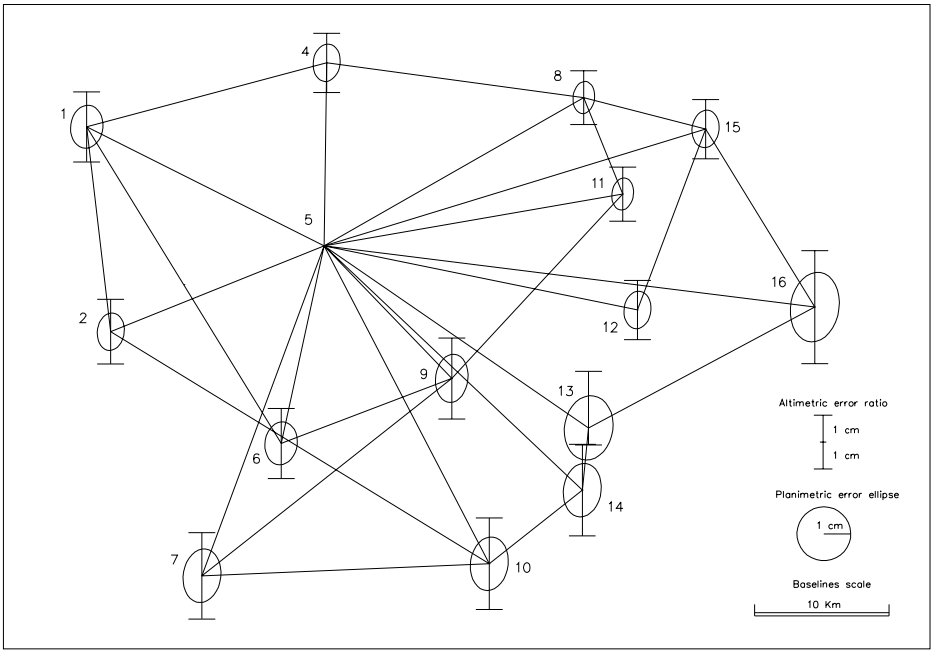

Fig. 5. Confidence regions from network adjustment in 1999 campaign.

the null hypothesis H_0 is accepted, and the coordinates differences show no significant change. On the contrary if,

$$F_{sp} > F_{m,(r_1+r_2),\alpha} = F_t \,, \tag{3}$$

the null hypothesis is rejected and it is possible to conclude that the coordinates have changed significantly.

To identify a point whose coordinates have changed it is necessary to test each point separately in turn (*Crespi, 1996*). To establish the final datum, i.e. to find the stable points, it is necessary to use an iterative procedure. First, each point is tested to define a starting datum including only the point *i* for which the statistics (1) is minimum. Next, the coordinate differences and their covariance matrix in the current datum are computed. Then, new test on each point to choose other point *j* to be included in the datum is carried out for which hypothesis H_0 is accepted: $F_{sp(j)} \le F_{m_K,(r_1+r_2),\alpha}$ where m_j is the number of point *j* coordinates tested. At the first iteration all points except the fixed point *i* are tested. The procedure continues starting again in the second step and stops when the datum cannot be enlarged.

It is important to stress that a complete spatial rotation between the two sets of coordinates taking into account their full covariance matrices should be estimated to reduce the coordinates to the same reference frame before testing the statistical significance of the coordinate differences.

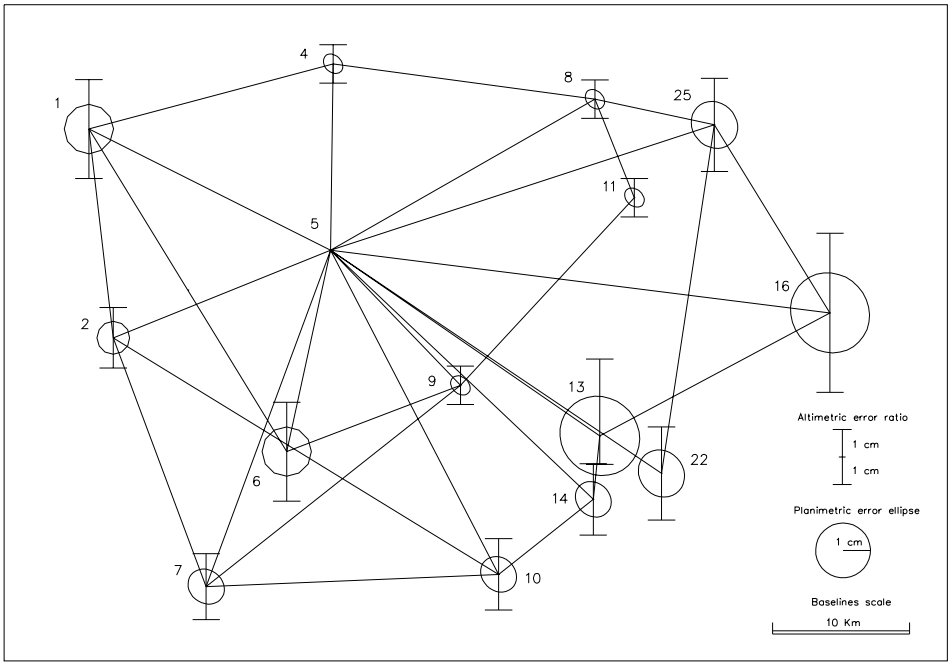

Fig. 6. Confidence regions from network adjustment in 2000 campaign.

The DENETGPS program (*Crespi, 1996*) has been used to evaluate the significance of the coordinates differences from Tables 2 and 3, without assuming any initial hypothesis on the points behaviour or any geophysical constraint. This assumption corresponds to fix the centroid of the whole network. All the points except #1 do not have significant coordinate changes at 5% significance level (Fig. 7).

5. CONCLUSIONS

Geological and seismological data indicate that, at present, the Granada Basin is subjected to NW-SE compression and a linked NE-SW extension. The NE-SW extension is accommodated by NW-SE normal faults, which are mainly concentrated in the NE sector of the Basin. In the studied sector, the marine Tortonian rocks, cut by these active faults, are located at different altitudes. Using these Tortonian rocks as a stratigraphic marker we have estimated a total throw of 2200 m along a 15 km studied segment. From the estimated throw we obtain a minimum extensional rate of 0.15 – 0.30 mm/year along the NE-SW segment, assuming a fault dip varying between 45º and 60º. This is a minimum value because: (1) extension is accompanied by block rotation, (2) faults have a probable listric geometry and (3) although the active faults at the studied sector (NE of the Basin), are mainly concentrated at the surface, seismicity is distributed over the whole Basin.

Table 2. Cartesian Coordinates at epoch 1999.2 in ITRF97 [m]

Point	*X*	*RMS*	*Y*	*RMS*	*Z*	*RMS*
1	5072188.505	0.006	–358004.647	0.002	3838676.875	0.004
2	5081674.060	0.006	–356735.530	0.002	3826736.459	0.004
4	5070601.070	0.005	–340077.136	0.002	3842757.716	0.004
5	5078620.539		–340687.296		3831772.511	
6	5087664.178	0.006	–344352.944	0.002	3820335.237	0.004
7	5093135.067	0.007	–350540.206	0.003	3812385.160	0.005
8	5073317.931	0.005	–321073.917	0.002	3840788.977	0.003
9	5085275.191	0.007	–331516.393	0.003	3824101.271	0.005
10	5094239.385	0.008	–329194.046	0.003	3813504.882	0.006
11	5077851.771	0.005	–318413.095	0.002	3835122.567	0.003
12	5083016.829	0.005	–317561.799	0.002	3828201.000	0.004
13	5088411.593	0.009	–321496.156	0.004	3821432.539	0.007
14	5090886.351	0.008	–322090.759	0.003	3817537.778	0.006
15	5075598.725	0.005	–312127.606	0.002	3839237.978	0.004
16	5084740.691	0.009	–304463.328	0.004	3829269.292	0.007

Table 3. Cartesian Coordinates at epoch 2000.5 in ITRF97 [m].

Point	*X*	*RMS*	*Y*	*RMS*	*Z*	*RMS*
1	5072188.512	0.008	–358004.626	0.004	3838676.867	0.006
2	5081674.060	0.005	–356735.528	0.002	3826736.456	0.004
4	5070601.075	0.003	–340077.129	0.001	3842757.739	0.002
5	5078620.539		–340687.296		3831772.511	
6	5087664.169	0.008	–344352.943	0.004	3820335.233	0.006
7	5093135.071	0.006	–350540.205	0.003	3812385.159	0.004
8	5073317.940	0.003	–321073.919	0.001	3840788.999	0.002
9	5085275.189	0.003	–331516.398	0.001	3824101.280	0.002
10	5094239.391	0.006	–329194.052	0.003	3813504.893	0.004
11	5077851.785	0.003	–318413.099	0.001	3835122.585	0.002
22	5090009,993	0.008	–317065.680	0.003	3819061.129	0.005
13	5088411.604	0.012	–321496.158	0.006	3821432.553	0.009
14	5090886.382	0.006	–322090.760	0.003	3817537.807	0.004
25	5075254.333	0.007	–312127.714	0.003	3839237.522	0.005
16	5084740.720	0.013	–304463.326	0.006	3829269.315	0.010

A GPS monitoring network has been established and the first two campaigns have been compared. A statistical procedure has been used to evaluate the significance of the coordinates differences without assuming any initial hypothesis on the point's behaviour or any geophysical constraint. All the points except one show no significant coordinates changes at the 5% significance level, which agrees with the low rate of extension calculated from geological data. The reoccupation campaign carried out a year after the

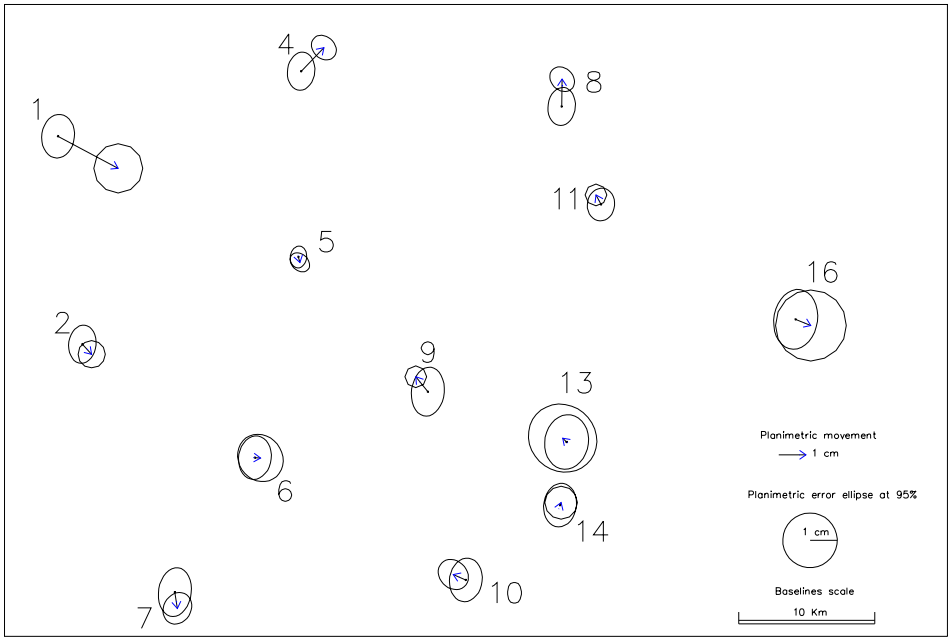

Fig. 7. Displacement vectors of all points in the frame of final datum and 95% reliability ellipses.

first campaign allows confirming that the rates are small. In order to detect such small rates, one has to have observations over a longer time span, probably a decade.

The studied region has some particularities that will be clarified in the future, because focal mechanism and regional information show a NW-SE compression together with NE-SW extension, but local geological information only brings out a NE-SW extension. The present and future results will be very significant to have a good knowledge of the recent movements and to obtain velocities of the main faults. Moreover, the movements that will be obtained in future campaigns probably will clarify the controversy between the fact that in this area all the faults are normal in appearance, but focal mechanism and regional stress field indicate a strike slip regime.

Acknowledgements: The authors gratefully acknowledge the support given by *Dirección General de Enseñanza Superior e Investigación Científica* (Spain) (Project PB97-1267-C03). Thanks are due to the reviewers for their helpful comments.

Received: October 29, 2001; *Accepted: January 24, 2002*

References

Alfaro P., Galindo-Zaldívar J., Jabaloy J., López-Garrido A.C. and Sanz de Galdeano C., 2001. Paleoseismic evidences in the Padul area (south of Granada, Betic Cordillera). *Acta Geológica Hispánica*, **36**(3–4), 283–295.

Argus D.F., Gordon R.G., De Mets C. and Stein S., 1989. Closure of the Africa-Eurasia-North America plate motion circuit and tectonics of the Gloria Fault. *J. Geophys. Res.*, **94**, 5585–5602.

Betti B., Biagi L., Crespi M. and Riguzzi F., 1999. GPS Sensitivity Analysis Applied to non-permanent Deformation Control Networks. *J. Geodesy*, **73(3)**, 158–167.

Calvache M.L., Viseras C. and Fernández J., 1997. Controls on fan development-evidence from fan morphometry and sedimentology; Sierra Nevada, SE Spain. *Geomorphology*, **21**, 69–84.

Crespi M., 1996. Software Package for the Adjustment and the Analysis of GPS Control Networks. In: M. Unguendoli (ed.), *Reports on Survey and Geodesy in memoria of Proff. A. Gubellini and G. Folloni.* Edizione Nautilus, Bologna, 237–264.

Crespo-Blanc A., García-Dueñas V. and Orozco M., 1993a. Systèmes en extension dans la Chaîne Bétique Centrale: que reste-t-il de la structure en nappes du complexe Alpujarride?. *C.R. Acad. Sc. Paris*, **317(II)**, 971–977 (in French).

Crespo-Blanc A., Orozco M. and García-Dueñas V., 1993b. Extension versus compression during the Miocene tectonic evolution of the Betic Chain. Late folding of normal fault systems. *Tectonics*, **13**, 78–88.

DeMets C., Gordon R.G., Argus D.F. and Stein S., 1994. Effect of recent revisions to the geomagnetic reversal time scale on estimates of current plate motions. *Geophys. Res. Lett.*, **21**, 2191–2194.

Estévez A. and Sanz de Galdeano C., 1983. Néotectonique du secteur central des Chaînes Bétiques (Basins du Guadix-Baza et de Grenade). *Rev. Géogr. Phys. Géol. Dynam.*, **21**, 23–34 (in French).

Fontboté J.M., 1957. Tectoniques superposées dans la Sierra Nevada (Cordillères Bétiques, Espagne). *C.R. Acad.Sci. Paris*, **245**, 1324–1326 (in French).

Galindo-Zaldívar J., González-Lodeiro F. and Jabaloy A., 1989. Progressive extensional shear structures in a detachment contact in the Western Sierra Nevada (Betic Cordilleras, Spain). *Geodinamica Acta*, **3**, 73–85.

Galindo-Zaldívar J., Jabaloy A. and González-Lodeiro F., 1996. Reactivation of the Mecina detachment in the western sector of Sierra Nevada (Betic Cordilleras, SE Spain). *C.R. Acad. Sci. Paris*, **323(IIa)**, 615–622.

Galindo-Zaldívar J., Jabaloy A., Serrano I., Morales J., González-Lodeiro F. and Torcal F., 1999. Recent and present-day stresses in the Granada Basin (Betic Cordilleras): Example of a late Miocene-present-day extensional Basin in a convergent plate boundary. *Tectonics*, **18**, 686–702.

García-Dueñas V., Balanyá J.C. and Martínez-Martínez J.M., 1992. Miocene extensional detachments in the outcropping basement of the northern Alboran Basin (Betics) and their implications. *Geo-Marine Letters*, **12**, 88–95.

Klotz J. and Lelgemann D., 1999. Present State of the Central Anden GPS-Traverse ANSA. GPS Techniques Applied to Geodesy and Surveying. *Lectures Notes in Earth Sciences*, **19**, 427–436.

Lhénaff R., 1965. Néotectonique quaternaire sur le bord occidental de la Sierra Nevada (province de Grenade, Espagne). *Rev. Géogr. Phys. Géol. Dynam.*, **2(VII)**, 205–207 (in French).

Martínez-Martínez J.M. and Azañón J.M., 1997. Mode of extensional tectonics in the southeastern Betics (SE Spain): Implications for the tectonic evolution of the peri-Alborán orogenic system. *Tectonics*, **16**, 205–225.

Morales J., Serrano I., Vidal F. and Torcal F., 1997. The depth of the earthquake activity in the Central Betics (Southern Spain). *Geophys. Res. Lett.*, **24**, 3289–3292.

Muñoz D. and Udías A., 1991. Three large historical earthquakes in southern Spain. In: J. Mezcua and A. Udias (Eds.)., *Seismicity, Seismotectonics and Seismic Risk of the Ibero-Maghrebian Region. Monografías del Instituto Geográfico Nacional*, **8**, 175–182.

Riley C. and Moore J., 1993. Digital elevation modelling in a study of the neotectonic geomorphology of the Sierra Nevada, southern Spain. *Z. Geomorph. N.F.*, **94**, 25–39.

Rodríguez-Fernández J., 1982. *El Mioceno del sector central de las Cordilleras Béticas.* PhD thesis Univ. Granada, 224 pp. (in Spanish).

Rothacher M., Mervant L., Beutler G., Brockmann E., Fankhauser S., Gurtner W., Johnson J., Schaer S., Springer T. and Weber R., 1996. *BERNESE GPS software version 4.0*. Astronomical Institute, University of Bern.

Sanz de Galdeano C. and López-Garrido A.C., 1999. Nature and impact of the Neotectonic deformation in the western Sierra Nevada (Spain). *Geomorphology*, **30**, 259–272.

Sanz de Galdeano C. and López-Garrido A.C., 2000. Las fallas tortonienses a cuaternarias entre Granada y la costa: el límite occidental del nevado-filábride y de las unidades alpujárrides inferiores. *Rev. Soc. Geol. España*, **13(3-4)**, 519–528 (in Spanish).

Vidal F., 1986. *Sismotectónica de la región Béticas-Mar de Alborán*. Ph.D. Thesis, Universidad de Granada. 250 pp. (in Spanish).